frontiers | Frontiers in Chemistry

TYPE Original Research
PUBLISHED 12 August 2024
DOI 10.3389/fchem.2024.1459324

OPEN ACCESS

EDITED BY
Xifei Li,
Xi'an University of Technology, China

REVIEWED BY
Donglei Guo,
Luoyang Normal University, China
Di Zhao,
Beijing Institute of Technology, China

*CORRESPONDENCE
Xia Wang,
wangxiakuaile@qdu.edu.cn

RECEIVED 04 July 2024
ACCEPTED 18 July 2024
PUBLISHED 12 August 2024

CITATION
Sun Z, Wang Y, Xu J and Wang X (2024), Mo_3P/Mo heterojunction for efficient conversion of lithium polysulfides in high-performance lithium-sulfur batteries.
Front. Chem. 12:1459324.
doi: 10.3389/fchem.2024.1459324

Mo_3P/Mo heterojunction for efficient conversion of lithium polysulfides in high-performance lithium-sulfur batteries

Zhongpeng Sun, Yuanhao Wang, Jie Xu and Xia Wang*

College of Physics, Qingdao University, University-Industry Joint Center for Ocean Observation and Broadband Communication, Qingdao, China

Realizing efficient immobilization of lithium polysulfides (LiPSs) as well as reversible catalytic conversion between LiPSs and the insoluble Li_2S is vital to restrain the shuttle effect, which requires highly reactive catalysts for high-performance Li-S batteries. Here, three-dimensional ordered porous Mo-based metal phosphides (3DOP Mo_3P/Mo) with heterogeneous structures were fabricated and utilized as separator-modified coatings for Li-S batteries to catalyze the conversion of LiPSs. The adsorption, catalytic and electrochemical performance of the corresponding cells were compared among 3DOP Mo_3P/Mo and 3DOP Mo, by kinetic and electrochemical performance measurements. It was found that the cell with 3DOP Mo_3P/Mo modified separator deliver better electrochemical performance, with a high specific capacity of 469.66 mAh g^{-1} after 500 cycles at a high current density of 1°C. This work provides an idea and a guideline for the design of the separator modification for high-performance Li-S batteries.

KEYWORDS

lithium-sulfur batteries, three-dimensional ordered porous (3DOP) architecuture, heterogeneous structure, Mo_3P, Mo

Introduction

With the shortage of non-renewable energy sources such as traditional fossil fuels, the development of electrochemical energy storage systems with high energy density and long life is the key to increase the utilization of renewable energy sources. In recent years, lithium-sulfur (Li-S) batteries have received extensive research attention due to their high theoretical energy density (2,600 Wh kg^{-1}), cost-effectiveness, and environmental friendliness of sulfur (Robinson et al., 2021). However, Li-S batteries still face many obstacles, including the slow kinetics of lithium polysulfides (LiPSs) conversion during charging and discharging to cause the shuttling effect (Wang et al., 2023), associated with the volume expansion caused by sulfur phase transition. It is pivotal to address the above issues for accelerating the development of Li-S batteries (Wang et al., 2022; Chen et al., 2024).

Electrocatalysts have been reported to promote the conversion of LiPSs to improve the utilization of sulfur and cycling stability (Dai et al., 2021; Feng et al., 2022). Among the numerous catalysts, transition metal phosphides (TMPs) (Liu et al., 2023; Zhang et al., 2024), such as CoP (Sun et al., 2023), Ni_2P (Niu et al., 2023), etc. have been widely utilized in Li-S batteries to catalyze the reaction of LiPSs due to their good structural and thermal stability, along with abundant active sites. Especially, Mo_3P possesses low work function

accompanied by rich valence electrons in 3d orbitals, thus presenting very broad application prospects in boosting the conversion of LiPSs, which has scarcely been reported.

Generally, the conductivity of the molybdenum phosphide as a semiconductor material can not meet the requirements of an electrocatalyst perfectly (Feng et al., 2024). The combination of the molybdenum phosphide and materials good electrical conductivity, such as carbon, metal, etc. to form composited or heterogeneous materials has been regarded as an effective strategy to improve the conductivity and promote charge transfer (Yuan et al., 2017; Feng et al., 2023). For example, Li et al. designed the Co-CoP heterostructure to effectively confine and catalyze the conversion of LiPSs while enhancing ionic and electron migration. The volume expansion of LiPSs on NCNT@Co-CoP-1 was also significantly reduced at high S loading, and the catalytic conversion efficiency was improved (Li et al., 2021). Therefore, the design of metal phosphide/metal heterojunctions is crucial to further improve the performance of Li-S batteries.

In this work, we report for the first time the synthesis of three-dimensional ordered porous (3DOP) Mo_3P/Mo composites as separator-modified coatings by a sol-gel method to improve the electrochemical performance of Li-S batteries (Li et al., 2021; Li et al., 2021; Zhu et al., 2021). The material characterization, adsorption performance, and battery performance tests show that compared with the monometallic (Mo) modified separator, the heterostructured Mo_3P/Mo catalyst possesses a stronger interaction with Li_2S_6, which effectively restricts the shuttling effect of LiPSs, strengthens the electron transfer ability, improves the reaction kinetics of LiPSs, and further enhances the sulfur utilization, thus improving the cycling stability of Li-S batteries.

Experimental section

Preparation of 3DOP Mo_3P/Mo

Firstly, 0.741 g of $(NH_4)_2MoO_4$ were dissolved in 5 mL of deionised water (DI) under magnetic stirring, and then 0.0792 g of diammonium hydrogen phosphate $[(NH_4)_2HPO_4]$ was added. Subsequently, 0.252 g of $C_6H_5NO_4$ was added in the above solution and placed in an oil bath under 90°C until the solution became a gel. Afterwards, 1.56 g of SiO_2 was mixed with the gel, which was then dried in an oven. The dried sample was then calcined at 900°C for 6 h under Ar/H_2 gas. The final 3DOP structured product was obtained through etching SiO_2 using NaOH solution.

Preparation of 3DOP Mo

Firstly, 0.7062 g of $(NH_4)_2MoO_4$ were dissolved in 15 mL of deionised water (DI) under magnetic stirring, and then 2.446 g of $C_6H_5NO_4$ was added in the above solution and placed in an oil bath under 90°C until the solution became a gel. Afterwards, 1.56 g of SiO_2 was mixed with the gel, which was then dried in an oven. The dried sample was then calcined at 900°C for 8 h under Ar/H_2 gas. The final 3DOP structured product was obtained through etching SiO_2 using NaOH solution.

Materials characterization

The phase and purity of the resulting samples were analyzed by powder x-ray diffraction (XRD) (Rigaku D/Max X-ray diffractometer with Cu Kα radiation). Morphological images of the final products were obtained by scanning electron microscopy (SEM, JSM-6700F, JEOL). The surface elemental composition and chemical valence states of the product were determined by X-ray photoelectron spectroscopy (XPS, PHI-5702, Physical Electronics).

Synthesis of sulfur electrodes

The mixture of Ketjen black and sulfur powder with a mass ratio of 7:3 was ground for 30 min and heated at 155°C for 12 h under an Ar atmosphere. After cooling to room temperature, the sulfur cathode with 65% sulfur was obtained. Subsequently, the working electrodes named KB/S were prepared through casting the above homogeneous slurry, composed of KB/S, KB, and LA133 with a mass ratio of 7:2:1, on Al foil, followed by vacuum dried overnight at 60°C. Finally, the Al foil coated with KB/S was punched into disks with a diameter of 12 mm.

Assembly of Li-S batteries

Li-S cells were assembled using CR2032-type coin cells in the Ar-filled glove box employing the KB/S electrode as the cathode, Li as the anode, Celgard 2,400 as the separator, 3DOP Mo_3P/Mo as the separator interlayer and 1.0 M LiTFSI in a DME/DOL (v/v = 1/1) solution with 1 wt% $LiNO_3$ as the electrolyte. The areal sulfur loading of the cathode was around 1.3 mg cm^{-2} (E/S ratio: 50 μL mg^{-1}).

Electrochemical characterizations

Galvanostatic charge/discharge tests for Li-S cells wereacquired with the voltage ranging from 1.8 to 2.7 V (Neware, Shenzhen, China). Cyclic voltammetry (CV) and electrochemical impedance (EIS) measurements were collected on a CHI660 electrochemical workstation. And the CV profiles were conducted at a scanning rate of 0.1 mV s^{-1} from 1.8 to 2.7 V. Electrochemical impedance spectroscopy (EIS) data were performed by the same electrochemical workstation by applying a 1 mV amplitude signal from 100 kHz to 0.01 Hz. The galvanostatic intermittent titration technique (GITT) were conducted at a pulse current of 0.05°C, and the pulse time and relaxation time are both 30 min.

Adsorption test of LiPSs

Firstly, Li_2S_6 solution (2 mM) was obtained through vigorously stirring the mixed solution consisting of Li_2S and S dissolved in DOL + DME (v/v, 1:1) solvent with a molar ratio of 1:5. Afterwards, 3DOP Mo_3P/Mo and 3DOP Mo were separately placed into the above Li_2S_6 solution with 1 mL. After 6 h of adsorption, the supernatants were

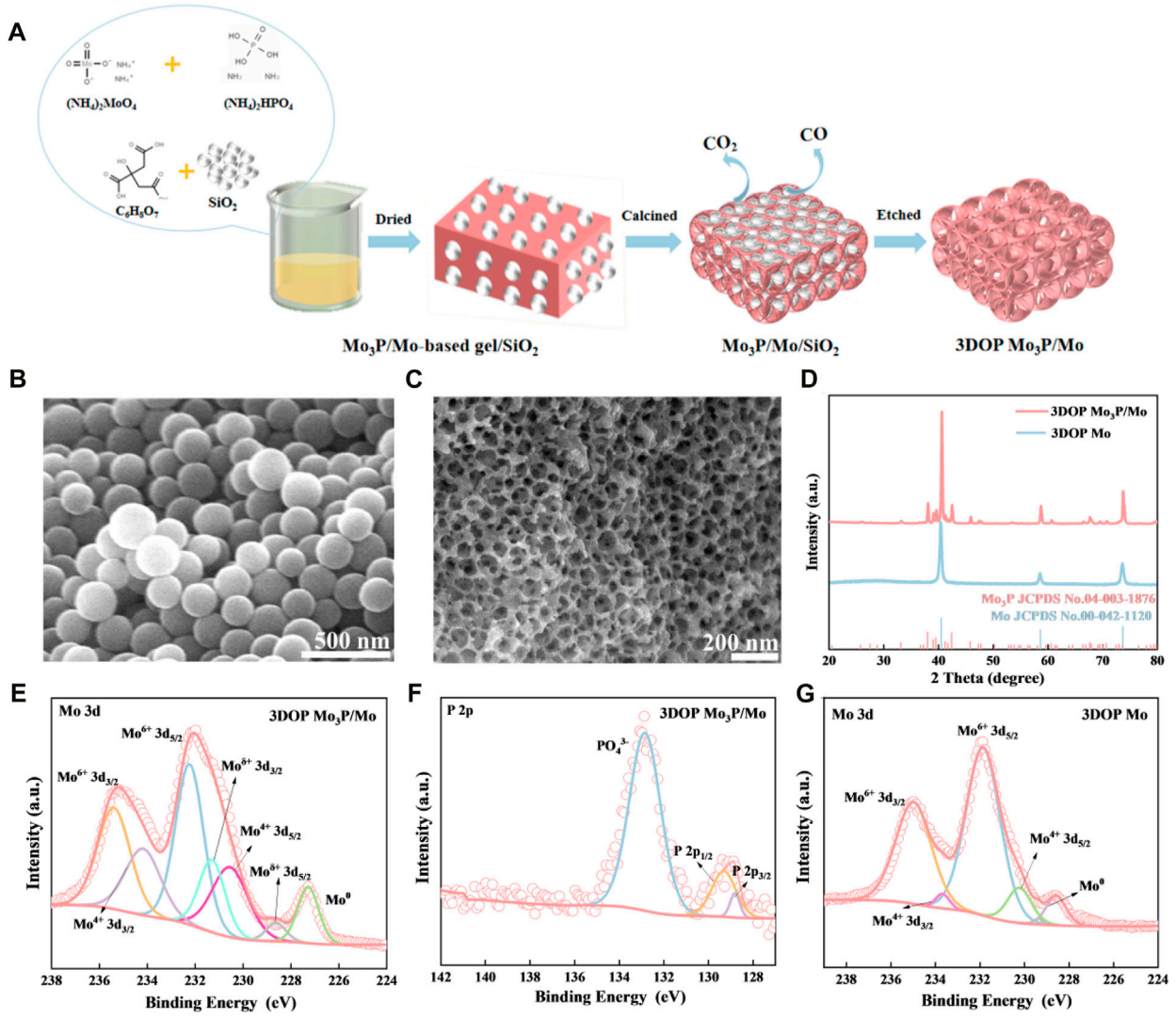

FIGURE 1
(A) Scheme of the synthesis process of 3DOP Mo_3P/Mo. **(B, C)** SEM images of SiO_2 templates and 3DOP Mo_3P/Mo, respectively. **(D)** XRD patterns of 3DOP Mo_3P/Mo and 3DOP Mo. High resolution XPS spectra of **(E)** Mo 3d and **(F)** P 2p in 3DOP Mo_3P/Mo. **(G)** High resolution XPS spectra of Mo 3d.

tested by ultraviolet spectrophotometer, and the four catalysts were measured using XPS.

Results and discussion

The novel 3DOP Mo_3P/Mo was fabricated and corresponding synthesized process was depicted in Figure 1A. Firstly, ammonium molybdate was mixed with diammonium hydrogen phosphate and then citric acid and SiO_2 spheres with average diameter size of around 150 nm (Figure 1B) were added to form a gel under oil bath, which was subsequently calcined to generate a Mo_3P/Mo/SiO_2 composite. After etching of SiO_2, the final sample was achieved with 3D ordered hierarchical porous architecture (Wang et al., 2018; Li et al., 2021), composed of ordered macropores with a diameter size of approximately 150 nm, consistent with SiO_2 spheres, and numerous meso-micropores caused by the decomposition of citric acid to generate gases, which was confirmed by the SEM image (Figure 1C).

Subsequently, the powder XRD patterns of the prepared 3DOP samples are shown in Figure 1D. All diffraction peaks of the prepared product are ascribed to Mo_3P (JCPDS No. 04-003-1876) and Mo (JCPDS No. 00-042-1120) in the absence of other impurities, revealing the formation of pure Mo_3P/Mo phase. Besides, the corresponding monometallic as comparison sample is also pure Mo (JCPDS No. 00-042-1120).

Additionally, the survey XPS spectrum (Supplementary Figure S1A) shows that the surface elements are mainly composed of Mo, P, C and O in the 3DOP Mo_3P/Mo material (Wu et al., 2023). The Mo 3d high-resolution scans, as shown in Figure 1E, the four main peaks presented at 235.4, 234.1, 232.2, and 230.5 eV belong to Mo^{6+} and Mo^{4+}, which are oxidized phases due to the oxidation of the 3DOP Mo_3P/Mo surface. The pair of peaks with binding energies of 231.3 and 228.6 eV corresponds to $Mo^{\delta+}$ ($0<\delta<4$) of Mo_3P and the peak at 227.3 eV is attributed to Mo^0. Meanwhile, the high resolution XPS spectrum of P 2p (Figure 1F) displays three main peaks at 132.9, 129, and 128 eV, belonging to PO_4^{3-}, $2p_{1/2}$ and $2p_{3/2}$.

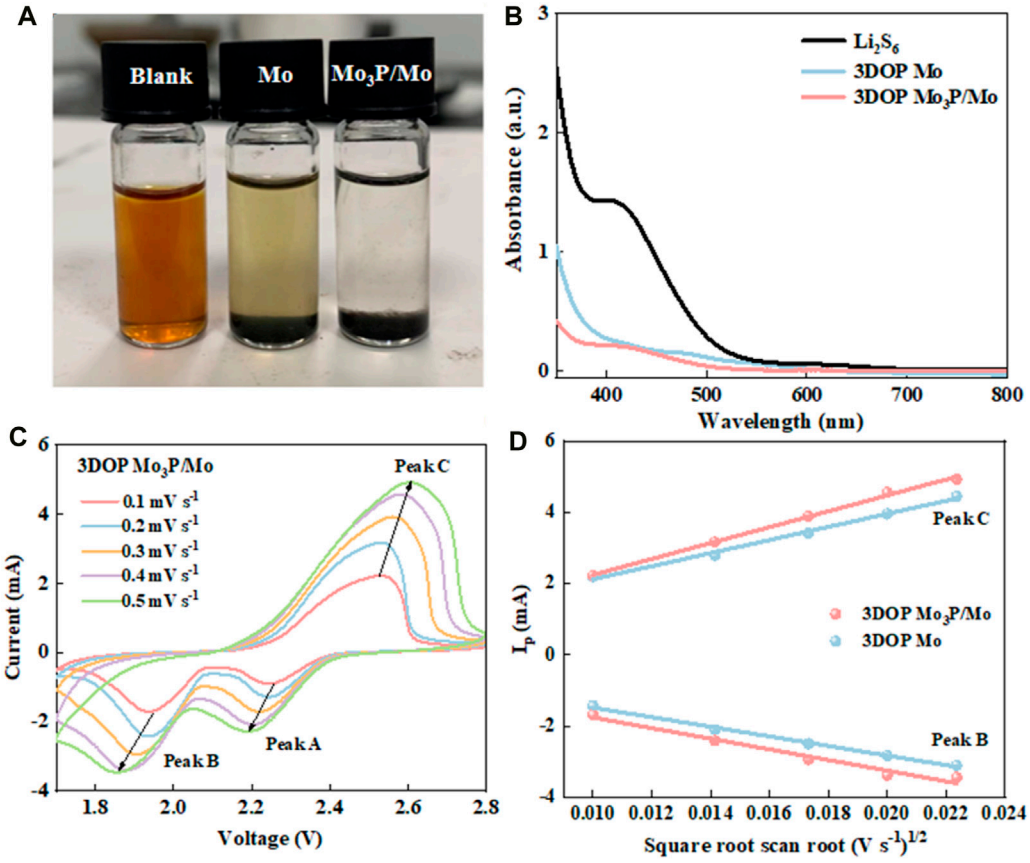

FIGURE 2
(A, B) Static lithium polysulfide adsorption tests and UV-vis absorption spectra of Li_2S_6 solutions after adding 3DOP Mo_3P/Mo and 3DOP Mo. **(C)** CV curves of 3DOP Mo_3P/Mo under different sweep speeds. **(D)** Linear fitting of peak currents *versus* square root scan rate of the as-synthesized catalysts.

In addition, the full spectrum and the valence distribution of 3DOP Mo are shown in Supplementary Figures S1B, G. The surface elements of the 3DOP Mo materials are mainly composed of Mo, C and O. There are four main peaks at 234.9, 233.6, 231.8, and 230.3 belonging to Mo^{6+} and Mo^{4+}, respectively, which are due to the surface oxidation in the high resolution Mo 3d spectrum, while the characteristic peak at around 228.2 eV corresponds to Mo^0.

In order to resolve the shuttle effect of LiPSs, the catalysts firstly are expected to be capable of achieving strong adsorption. Accordingly, in view of investigating the adsorption capability of 3DOP Mo_3P/Mo and 3DOP Mo, the adsorption visualization measurements for two samples and Li_2S_6 solutions (Wang et al., 2022; Huang et al., 2023). As shown in Figure 2A, the initial yellow color of Li_2S_6 solution becomes light for 3DOP Mo material, while the yellow Li_2S_6 solution contained 3DOP Mo_3P/Mo changes to nearly transparent after 6 h, suggesting the stronger adsorption capability of 3DOP Mo_3P/Mo towards LiPSs (Lei et al., 2018). Moreover, the solutions after visualization adsorption experiments were diluted and then measured using a UV–vis spectroscopy. The UV–vis spectra in Figure 2B show a lower peak of 3DOP Mo_3P/Mo compared with 3DOP Mo at around 420 nm, demonstrating the above conclusion (Xu et al., 2024).

The reaction kinetics of these two samples about the conversion of LiPSs were also further explored. Figure 2C and Supplementary Figure S2 show the CV curves of Li-S batteries assembled by 3DOP Mo_3P/Mo modified separator at different scan rates. In addition, the diffusion coefficients of each electrode were calculated based on these CV curves in Supplementary Figure S3 (Wang et al., 2022), which were calculated with the classical Randles-Sevcik Equation:

$$I_p = 2.69 \times 10^5 n^{3/2} A D_{Li^+}{}^{1/2} C_{Li^+} v^{1/2} \quad (1)$$

Thereinto, I_p and n represent the peak current and the number of electrons transferred, respectively. A is the active area of the electrode, D_{Li+} and C_{Li+} express the diffusion coefficient and concentration of Li^+, respectively, while v is the scan rate. According to the above formulation, the Li^+ diffusion coefficient is a positive correlation with the slopes of $v^{1/2}$ and I_p (Xu et al., 2022). As shown in Figure 2D, the Li-S battery assembled by 3DOP Mo_3P/Mo possesses the highest slope in both oxidation and reduction reactions, which suggests that 3DOP Mo_3P/Mo promotes charge transfer and significantly accelerates redox reaction kinetics (Wu et al., 2023).

To clarify the reason for good reaction dynamics of 3DOP Mo_3P/Mo, the electrochemical impedance spectroscopy (EIS) spectra of 3DOP Mo_3P/Mo and 3DOP Mo under various temperatures were measured, depicted in Figure 3A and Supplementary Figure S4 (Jiang et al., 2022). As is observed that all Nyquist plots mainly consist of a semicircle in the mid/high-frequency region as well as a straight line in the low-frequency region, corresponding to the charge transfer resistance (R_{ct}) as well as the ion diffusion impedance, respectively.

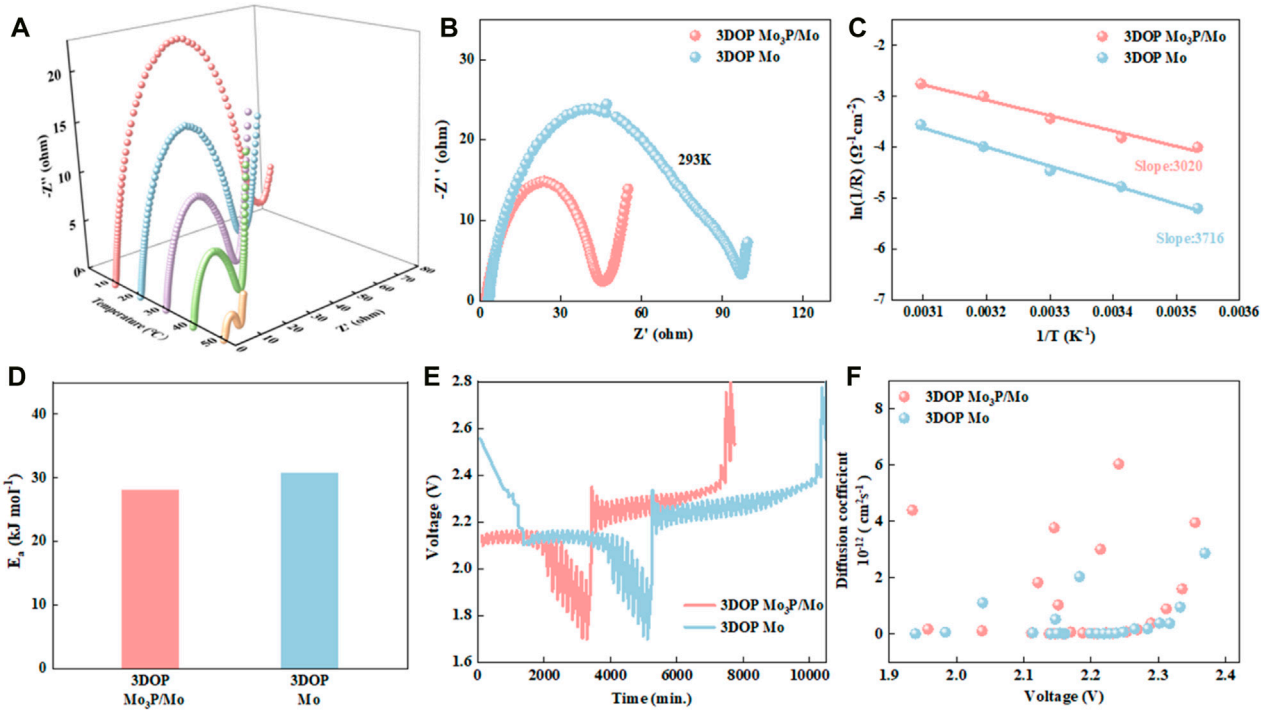

FIGURE 3
(A) EIS spectra of 3DOP Mo_3P/Mo at different temperatures. **(B)** Electrochemical impedance spectroscopy at 293 K. **(C)** Arrhenius plots of ln ($1/R_t$) vs.$1/T$ in 3DOP Mo_3P/Mo and 3DOP Mo-based batteries. **(D)** Activation energy (*Ea*) of 3DOP Mo_3P/Mo and 3DOP Mo. **(E)** GITT curves of 3DOP Mo_3P/Mo and 3DOP Mo at 40 mA g^{-1}. **(F)** Li^+ diffusion coefficients of 3DOP Mo_3P/Mo and 3DOP Mo.

In contrast with 3DOP Mo, 3DOP Mo_3P/Mo delivers a much smaller semicircle at each temperature (Figure 3B) (Hao et al., 2020; Zhao et al., 2020). Besides, activation energy (*Ea*) of 3DOP Mo_3P/Mo and 3DOP Mo materials required for chemical reactions was analyzed on the basis of Arrhenius equations (Figures 3C, D). 3DOP Mo_3P/Mo exhibits a lower E_a value of approximately 28.04 kJ mol^{-1}, in comparison with 3DOP Mo (30.84 kJ mol^{-1}), revealing that 3DOP Mo_3P/Mo is beneficial to speeding up the conversion reaction. In addition, the diffusion kinetics of Na^+ in 3DOP Mo_3P/Mo and 3DOP Mo was also further evaluated through galvanostatic intermittent titration technique (GITT) (Wang et al., 2023). Figures 3E, F depict the GITT time-potential curves at 40 mA g^{-1} with the corresponding Na^+ diffusion coefficients. As is clearly observed that the Na^+ diffusion coefficients (D_{Li+}) of 3DOP Mo_3P/Mo (6.033×10^{-12} - 3.387×10^{-16} cm^2 s^{-1}) are larger than those of 3DOP Mo (2.86×10^{-12} - 2.61×10^{-16} cm^2 s^{-1}), indicating that Li^+ is more beneficial to diffusing in 3DOP Mo_3P/Mo (Qi et al., 2023).

In order to investigate the electrochemical performance of Li-S batteries with 3DOP Mo_3P/Mo and 3DOP Mo as materials for diaphragms applied to Li-S batteries, button batteries were assembled with different samples of modified separators and electrochemically relevant tests were performed. In order to further investigate the polarization phenomenon during the redox process and the potential barriers for nucleation and dissolution of Li_2S, constant-current charge-discharge tests were carried out at a current density of 0.5 C. The charge-discharge curves are shown in Figure 4A (Zhou et al., 2020; Sun et al., 2024; Wu et al., 2024). The charge-discharge curves of the first cycle show that the two characteristic discharge platforms of the 3DOP Mo_3P/Mo battery are higher and flatter than those of the 3DOP Mo, and the corresponding capacity is also larger. The polarization voltages of 3DOP Mo_3P/Mo and 3DOP Mo cells were 265 mV and 304 mV (Tang et al., 2021; Zhao et al., 2021), respectively, which indicates that the 3DOP Mo_3P/Mo catalyst could better promote the conversion of LiPSs, and this result was in agreement with the CV curve data. What's more, the catalytic effect of 3DOP Mo_3P/Mo can be further explained by scrutinizing the voltage magnification plots. In general, the potential difference between the initial voltage and the tangent of the potential plateau for the conversion of Li_2S_4 to Li_2S_2 correlates with the ease of generating insoluble Li_2S_2/Li_2S, meaning a smaller potential difference represents a more likely occurrence of the reaction (Wu et al., 2022; Song et al., 2022). Figure 4B shows a partial enlargement of the discharge curve, which represents the conversion of LiPSs to insoluble Li_2S_2/Li_2S, where the voltage differences of 15.5 mV and 17.8 mV for 3DOP Mo_3P/Mo and 3DOP Mo cells, respectively, which demonstrates that soluble LiPSs (Li_2S_4) is more susceptible to the reaction catalyzed by 3DOP Mo_3P/Mo catalyzed is more easily converted to insoluble lithium sulfide (Li_2S_2/Li_2S) (Sun et al., 2023; Chen et al., 2024; Xiang et al., 2024).

Figure 4C shows the rate performance of the cells corresponding to 3DOP Mo_3P/Mo and 3DOP Mo. 3DOP Mo_3P/Mo cells possess specific capacities of 1529.77, 912.2, 848.34, 797.79 和 724.95 mAh g^{-1} at current densities of 0.2°C, 0.5°C, 1°C, 2°C, and 3°C (Xu et al., 2022), respectively, and their specific capacities can still recover to 975.44 mAh g^{-1} when the

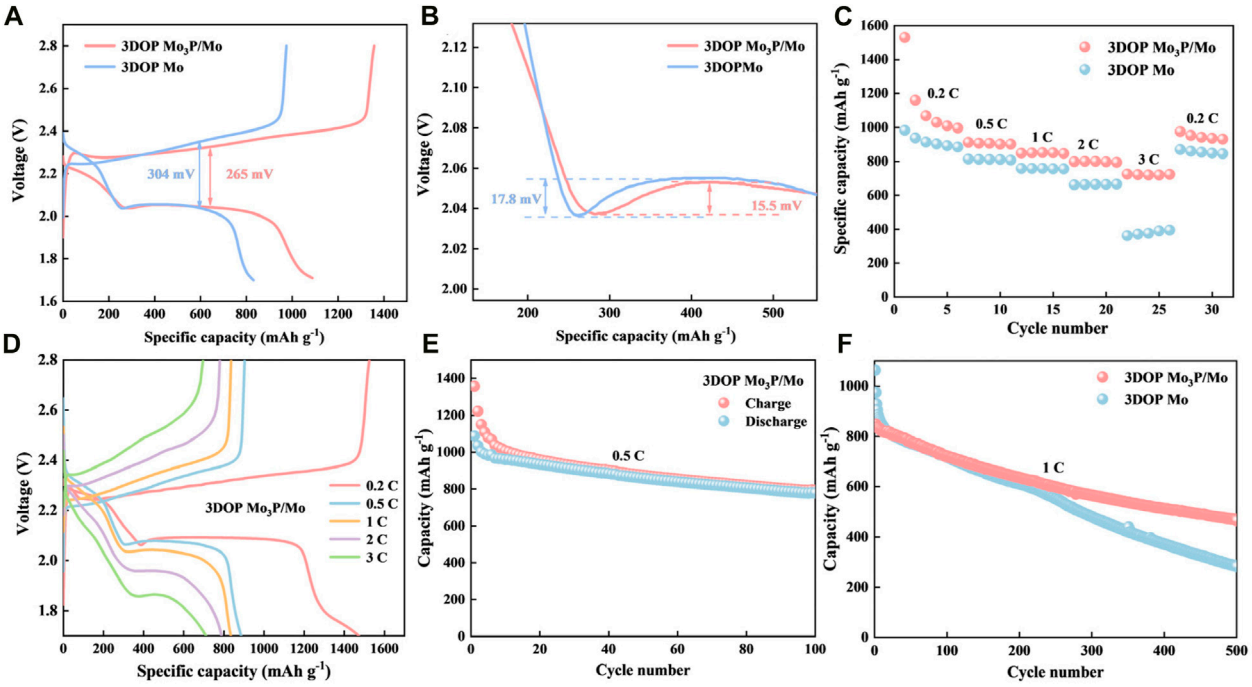

FIGURE 4
(A, B) Discharge–charge curves. **(C, D)** Rate performance of 3DOP Mo_3P/Mo and 3DOP Mo for Li-S batteries. **(E)** Cycling performances at 0.5°C of 3DOP Mo_3P/Mo. **(F)** Cycling performances at 1°C of 3DOP Mo_3P/Mo and 3DOP Mo.

current density returns to 0.2°C (Wang et al., 2023). When the current density was restored to 0.2°C, the specific capacity could still be restored to 975.44 mAh g^{-1}, indicating that the 3DOP Mo_3P/Mo cells deliver good rate performance compared to 3DOP Mo, which was attributed to the fact that 3DOP Mo_3P/Mo could better promote the cell's internal electrochemical processes. Figure 4D and Supplementary Figure S5 shows the charge/discharge curves of the two materials at different current densities (Guo et al., 2022), and even at high current densities, the 3DOP Mo_3P/Mo cell still shows a basic reaction plateau, which again indicates a faster electrochemical reaction. Figure 4E shows that 3DOP Mo_3P/Mo possesses high initial discharge and charge capacities of around 1357 and 1087 mAh g^{-1}, respectively, and stable capacity of 795 mAh g^{-1} after 100 cycles at 0.5°C (Guan et al., 2023). In addition, even at a high current density of 1°C, 3DOP Mo_3P/Mo provided a higher specific capacity of 469.66 mAh g^{-1} after 500 cycles compared to 3DOP Mo (283.33 mAh g^{-1}) (Figure 4F) (Wu et al., 2023), which suggests that the metallic phosphides/Mo heterostructuredemonstrate long cycle life and high specific capacity.

Conclusion

In summary, in this work, a three-dimensional porous Mo_3P/Mo heterostructure was successfully designed as a novel multifunctional catalyst for Li-S batteries. 3DOP Mo_3P/Mo possesses a strong adsorption for LiPSs and rapid transfer of internal electrons, which promoted the conversion of LiPS to effectively inhibit the shuttle effects. The results showed that the lithium-sulfur battery using 3DOP Mo_3P/Mo as the diaphragm could provide a high reversible capacity of up to 469.6 mAh g^{-1} after 500 cycles at 1°C. This work presents a new idea for the design of multifunctional electrocatalysts with molybdenum-based heterostructures for lithium-sulfur battery.

Data availability statement

The datasets presented in this study can be found in online repositories. The names of the repository/repositories and accession number(s) can be found in the article/Supplementary Material.

Author contributions

ZS: Writing–original draft. YW: Writing–original draft. JX: Writing–original draft. XW: Writing–review and editing.

Funding

The author(s) declare that financial support was received for the research, authorship, and/or publication of this article. National Key R&D Program of China with grant No. 2023YFF0720500, National Key Project with Grant No. 22-05-CXZX-04-03-15, National Nature Science Foundation of China (Nos 51871127 and 11674187) and Shandong Natural Science Foundation (No. ZR2022ME171).

Conflict of interest

The authors declare that the research was conducted in the absence of any commercial or financial relationships that could be construed as a potential conflict of interest.

Publisher's note

All claims expressed in this article are solely those of the authors and do not necessarily represent those of their affiliated organizations, or those of the publisher, the editors and the reviewers. Any product that may be evaluated in this article, or claim that may be made by its manufacturer, is not guaranteed or endorsed by the publisher.

Supplementary material

The Supplementary Material for this article can be found online at: https://www.frontiersin.org/articles/10.3389/fchem.2024.1459324/full#supplementary-material

References

Chen, L., Huang, L., Men, X., Bai, Y., Li, X., Li, Y., et al. (2024). Modified electron structure of CNT-$CoSe_2$ (vs. $CoSe_2$) with more Co^{2+} for improving catalytic effect in lithium sulfur batteries. *Mat. Today Commun.* 39, 108646. doi:10.1016/j.mtcomm.2024.108646

Chen, R., Zhou, Y., and Li, X. (2024). Nanocarbon-enabled mitigation of sulfur expansion in lithium–sulfur batteries. *Energy Storage Mat.* 68, 103353. doi:10.1016/j.ensm.2024.103353

Dai, H., Wang, L., Zhao, Y., Xue, J., Zhou, R., Yu, C., et al. (2021) "Recent advances in molybdenum-based materials for lithium-sulfur batteries. *Research* 2021, 5130420. doi:10.34133/2021/5130420

Feng, J., Liu, W., Shi, C., Zhang, C., Zhao, X., Wang, T., et al. (2024). Enabling fast diffusion/conversion kinetics by thiourea-induced wrinkled N, S co-doped functional MXene for lithium-sulfur battery. *Energy Stor. Mat.* 67, 103328. doi:10.1016/j.ensm.2024.103328

Feng, J., Shi, C., Dong, H., Zhang, C., Liu, W., Liu, Y., et al. (2023). Design of ZnSe-CoSe heterostructure decorated in hollow N-doped carbon nanocage with generous adsorption and catalysis sites for the reversibly fast kinetics of polysulfide conversion. *J. Energy Chem.* 86, 135–145. doi:10.1016/j.ensm.2024.103328

Feng, T., Zhao, T., Zhang, N., Duan, Y., Li, L., Wu, F., et al. (2022). 2D amorphous Mo-doped CoB for bidirectional sulfur catalysis in lithium sulfur batteries. *Adv. Funct. Mat.* 32 (30), 2202766. doi:10.1002/adfm.202202766

Guan, K., Yu, Y., Liu, H., Luo, J., Lei, W., and Zhang, H. (2023). Design of Co-doped hollow multi-channel carbon fibers for high performance lithium sulfur batteries. *Appl. Surf. Sci.* 638, 157963. doi:10.1016/j.apsusc.2023.157963

Guo, Y., Wu, P., Zhong, H., Huang, J., Ma, G., Xu, Z., et al. (2022). Prussian blue analogue/KB-derived Ni/Co/KB composite as a superior adsorption-catalysis separator modification material for Li-S batteries. *J. Colloid Interface Sci.* 625, 425–434. doi:10.1016/j.jcis.2022.06.036

Hao, Q., Cui, G., Zhang, Y., Li, J., and Zhang, Z. (2020). Novel $MoSe_2/MoO_2$ heterostructure as an effective sulfur host for high-performance lithium/sulfur batteries. *Chem. Eng. J.* 381, 122672. doi:10.1016/j.cej.2019.122672

Huang, M., Jiang, X., Xu, C., Zhao, S., Zhang, S., and Li, G. (2023). $CoMoO_4$ nanorods coated separator for high-performance lithium sulfur batteries. *Mat. Chem. Phys.* 295, 127182. doi:10.1016/j.matchemphys.2022.127182

Jiang, X., Zhang, S., Zou, B., Li, G., Yang, S., Zhao, Y., et al. (2022). Electrospun CoSe@NC nanofiber membrane as an effective polysulfides adsorption-catalysis interlayer for Li-S batteries. *Chem. Eng. J.* 430, 131911. doi:10.1016/j.cej.2021.131911

Lei, T., Chen, W., Hu, Y., Lv, W., Lv, X., Yan, Y., et al. (2018). A nonflammable and thermotolerant separator suppresses polysulfide dissolution for safe and long-cycle lithium-sulfur batteries. *Adv. Energy Mat.* 8 (32), 1802441. doi:10.1002/aenm.201802441

Li, C., Liu, R., Xiao, Y., Cao, F., and Zhang, H. (2021). Recent progress of separators in lithium-sulfur batteries. *Energy Stor. Mat.* 40, 439–460. doi:10.1016/j.ensm.2021.05.034

Li, J., Xie, W., Zhang, S., Xu, S.-M., and Shao, M. (2021). Boosting the rate performance of Li–S batteries under high mass-loading of sulfur based on a hierarchical NCNT@ Co-CoP nanowire integrated electrode. *J. Mat.* 9 (18), 11151–11159. doi:10.1039/d1ta00959a

Li, X., Han, Z., Yang, W., Li, Q., Li, H., Xu, J., et al. (2021). 3D ordered porous hybrid of ZnSe/N-doped carbon with anomalously high Na^+ mobility and ultrathin solid electrolyte interphase for sodium-ion batteries. *Adv. Funct. Mat.* 31 (50), 2106194. doi:10.1002/adfm.202106194

Liu, L., Yin, X., Li, W., Wang, D., Duan, J., Wang, X., et al. (2023). Transition metal phosphides: the rising star of lithium–sulfur battery cathode host. *Small* 20, 2308564. doi:10.1002/smll.202308564

Niu, Y., Feng, W., Lei, Z., Hu, W., Zheng, X., Su, W., et al. (2023). MXene surface-attached Ni_2P on lithium-sulfur battery catalytic effect. *J. Electroanal.* 946, 117743. doi:10.1016/j.jelechem.2023.117743

Qi, X., Huang, L., and Chen, Y. (2023). Superfine SnO_{2-x} particles embedded in a porous carbon matrix as a separator-modifying material for high-performance lithium sulfur batteries. *Ind. Eng. Chem. Res.* 62 (23), 9233–9245. doi:10.1021/acs.iecr.3c00655

Robinson, J. B., Xi, K., Kumar, R. V., Ferrari, A. C., Au, H., Titirici, M.-M., et al. (2021). 2021 roadmap on lithium sulfur batteries. *J. Phys. Energy* 3 (3), 031501. doi:10.1088/2515-7655/abdb9a

Song, H., Li, T., He, T., Wang, Z., Fang, D., Wang, Y., et al. (2022). Cooperative catalytic Mo-S-Co heterojunctions with sulfur vacancies for kinetically boosted lithium-sulfur battery. *Chem. Eng. J.* 450, 138115. doi:10.1016/j.cej.2022.138115

Sun, C., Han, Z., Wang, X., Liu, B., Li, Q., Li, H., et al. (2023). Advanced carbons nanofibers-based electrodes for flexible energy storage devices. *Adv. Funct. Mat.* 33 (52), 2305606. doi:10.1002/adfm.202305606

Sun, R., Qu, M., Peng, L., Yang, W., Wang, Z., Bai, Y., et al. (2023). Regulating electrochemical kinetics of CoP by incorporating oxygen on surface for high-performance Li–S batteries. *Small* 19 (41), 202302092. doi:10.1002/smll.202302092

Sun, X., Wang, X., Xiang, L., Wang, Y., Wang, Y., Li, N., et al. (2024). Excellent sodium metal deposition enabled by three-dimensional porous structures with natrophilic Ni-Sn alloy. *Appl. Phys. Lett.* 124 (16). doi:10.1063/5.0197966

Tang, Y., Huang, Y., Luo, L., Fan, D. E., Lu, Y., and Manthiram, A. (2021). Self-supported MoO_2/MoS_2 nano-sheets embedded in a carbon cloth as a binder-free substrate for high-energy lithium–sulfur batteries. *Electrochim. Acta* 367, 137482. doi:10.1016/j.electacta.2020.137482

Wang, J., Wang, H., Jia, S., Zhao, Q., Zheng, Q., Ma, Y., et al. (2023). Recent advances in inhibiting shuttle effect of polysulfide in lithium-sulfur batteries. *J. Energy Storage* 72, 108372. doi:10.1016/j.est.2023.108372

Wang, J., Wu, Z.-Y., Zhong, X.-N., Li, Y., and Han, S. (2022). Ni-NiS heterojunction composite-coated separator for high-performance lithium sulfur battery. *Coatings* 12 (10), 1557. doi:10.3390/coatings12101557

Wang, L., Wang, F., Zhu, J., Zhang, X., Tang, Y., and Wang, X. (2018). Synthesis and electrochemical performance of three-dimensional ordered hierarchically porous $Li_4Ti_5O_{12}$ for high performance lithium ion Batteries. *Ceram. Int.* 44 (2), 1296–1303. doi:10.1016/j.ceramint.2017.08.043

Wang, Q., Qin, B., Jiang, Q., Wang, B., Chen, Y., Yao, W., et al. (2023). Highly dispersed conductive and electrocatalytic mediators enabling rapid polysulfides conversion for lithium sulfur batteries. *Chem. Eng. J.* 476, 146865. doi:10.1016/j.cej.2023.146865

Wang, W., Xi, K., Li, B., Li, H., Liu, S., Wang, J., et al. (2022). A sustainable multipurpose separator directed against the shuttle effect of polysulfides for high-performance lithium–sulfur batteries. *Adv. Energy Mat.* 12 (19), 2200160. doi:10.1002/aenm.202200160

Wang, Z., Ma, Y., Song, J., Xu, X., Wu, Y., Wang, X., et al. (2023). Multiple heterostructures of Co and derivatives decorated high N-doped biochar host accelerating polysulfide redox kinetics for lithium sulfur batteries. *J. Alloys Compd.* 968, 171920. doi:10.1016/j.jallcom.2023.171920

Wu, C., Qi, G., Zhang, J., Cheng, J., and Wang, B. (2023). Porous Mo_3P/Mo nanorods as efficient mott-Schottky cathode catalysts for low polarization Li-CO_2 battery. *Small* 19 (44), 2302078. doi:10.1002/smll.202302078

Wu, N., Zhao, Z., Hua, R., Wang, X., Zhang, Y., Li, J., et al. (2024). Pre-doping of dual-functional sodium to weaken Fe─S bond and stabilize interfacial chemistry for high-rate reversible sodium storage. *Adv. Energy Mat.* 22, 2400371. doi:10.1002/aenm.202400371

Wu, S., Shi, J., Nie, X., Yu, Z., and Huang, F. (2022). Multi-duties for one post: biodegradable bacterial cellulose-based separator for lithium sulfur batteries. *Carbohydr. Polym.* 285, 119201. doi:10.1016/j.carbpol.2022.119201

Wu, T., Dou, H., Zhao, Z., Zhou, J., and Wang, X. (2023). Mo and Ni coordinated bimetallic oxide as catalyst in modified separators for low-capacity decay lithium sulfur batteries. *Chem. Nano. Mat.* 9 (7), e202300087. doi:10.1002/cnma.202300087

Xiang, L., Yang, W., Wang, Y., Sun, X., Xu, J., Cao, D., et al. (2024). Layered $BaV_6O_{16}{\cdot}3H_2O$@GO as a high performance cathode material for calcium ion batteries. *Chem. Commun.* 60 (41), 5459–5462. doi:10.1039/d4cc00988f

Xu, G., Gao, S., Song, X., Jiang, Y., and Zhang, X. (2022). Nitrogen-doped ordered multi-hollow layered carbon embedded with Mo_2C as lithium polysulfide restrained cathode for Li-S batteries. *Appl. Surf. Sci.* 574, 151634. doi:10.1016/j.apsusc.2021.151634

Xu, G., Li, R., Li, M., Zhang, Q., Li, B., Guo, J., et al. (2022). Rapid internal conversion harvested in Co/Mo dichalcogenides hollow nanocages of polysulfides for stable Lithium-Sulfur batteries. *Chem. Eng. J.* 434, 134498. doi:10.1016/j.cej.2022.134498

Xu, H., Jiang, Q., Shu, Z., Hui, K. S., Wang, S., Zheng, Y., et al. (2024). Fundamentally manipulating the electronic structure of polar bifunctional catalysts for lithium-sulfur batteries: heterojunction design versus doping engineering. *Adv. Sci.* 2307995, e2307995. doi:10.1002/advs.202307995

Yuan, H., Chen, X., Zhou, G., Zhang, W., Luo, J., Huang, H., et al. (2017). Efficient activation of Li_2S by transition metal phosphides nanoparticles for highly stable lithium–sulfur batteries. *ACS Energy Lett.* 2 (7), 1711–1719. doi:10.1021/acsenergylett.7b00465

Zhang, H., Han, G., Liu, Y., Zhao, L., Zhang, W., Khalil, M. T., et al. (2024). CoP/Co heterojunction on porous g-C_3N_4 nanosheets as a highly efficient catalyst for hydrogen generation. *J. Colloid Interf. Sci.* 658, 22–31. doi:10.1016/j.jcis.2023.12.044

Zhao, D., Qin, J., Zheng, L., Guo, D., Wang, J., and Cao, M. (2021). Covalent interfacial coupling of vanadium nitride with nitrogen-rich carbon textile boosting its lithium storage performance as binder-free anode. *Nano Res.* 14, 4336–4346. doi:10.1007/s12274-021-3853-6

Zhao, D., Sun, K., Cheong, W. C., Zheng, L., Zhang, C., Liu, S., et al. (2020). Synergistically interactive pyridinic-N–MoP sites: identified active centers for enhanced hydrogen evolution in alkaline solution. *Angew. Chem.* 132 (23), 9067–9075. doi:10.1002/ange.201908760

Zhou, X., Li, L., Yang, J., Xu, L., and Tang, J. (2020). Cobalt and molybdenum carbide nanoparticles grafted on nitrogen-doped carbon nanotubes as efficient chemical anchors and polysulfide conversion catalysts for lithium-sulfur batteries. *Chem. Electro. Chem.* 7 (18), 3767–3775. doi:10.1002/celc.202000909

Zhu, P., Gastol, D., Marshall, J., Sommerville, R., Goodship, V., and Kendrick, E. (2021). A review of current collectors for lithium-ion batteries. *J. Power Sources* 485, 229321. doi:10.1016/j.jpowsour.2020.229321